Perturbation Solutions of Unsteady Transonic Flow over Bodies of Revolution

Tsuying Hsieh*
Sverdrup/ARO, Inc., Arnold Air Force Station, Tenn.

A perturbation theory and numerical solution, based on the unsteady full potential equation, were developed for unsteady transonic flow about blunt and pointed bodies of revolution undergoing harmonic oscillations. The oscillatory motion was considered to be a small perturbation of the nonlinear steady flow. The coupled equations fo the mean steady and unsteady potentials were solved numerically using a rotating difference scheme. Calculations were performed for ogive-cylinder, ellipse-cylinder, hemisphere-cylinder, and parabolic arc nose shapes undergoing pulsatile and pitching oscillations. Comparisons of the present theory with available experiments and other theories are presented for the surface pressure distribution at quasi-steady state and for the static and dynamic stability derivatives.

I. Introduction

UNSTEADY transonic flow over bodies has been treated with linear differential equations for high reduced frequencies with major interest in obtaining stability derivatives for flutter analysis.[1] Since the range of engineering interest in the transonic flow regime is the low-frequency range, where the linearized equation breaks down, the nonlinear equation must be used. For slender bodies of revolution at zero incidence with a sharp nose, several investigators have developed approximate methods to solve the transonic small disturbance equation.[2-4] For blunt-nose bodies of revolution, these aforementioned methods are not applicable. In engineering applications, a method that can be applied to both blunt and pointed bodies of revolution is most desirable, and such a method is developed in this paper.

The method to be described is based on the numerical method developed by South and Jameson,[5] who solved the steady, full potential equation for axisymmetrical flow over blunt and pointed bodies of revolution at transonic speeds. Their methods shows good agreement with other theoretical methods and experiments at steady state.[6] Thus an extension of South and Jameson's scheme to calculate unsteady transonic flow has been pursued.

Among the harmonically oscillating motions for bodies of revolution, pitching oscillation has great engineering applications. However, once the body is at incidence, the flowfield is three-dimensional in nature. Numerical computation of exact three-dimensional transonic flow problems generally requires large amounts of computer storage and time and cannot be routinely employed in engineering applications. Therefore, an approximate method is sought. To obtain the stability derivatives for a body of revolution at zero incidence a small amplitude pitching motion may be assumed and cosine variation of flow quantities in the crossflow plane may be a valid approximation. Thus three-dimensional computation may be avoided.

The problem can be further simplified by introducing the perturbation approach. Because the unsteady motion is assumed to be small amplitude oscillation, the flow may be divided into mean steady and unsteady components, with the latter as a perturbation of the former. (This assumption is similar to those of Refs. 1-4 for the sharp-nose body of revolution and has been used in many analyses of transonic flow over oscillating airfoils based on transonic small disturbance equations, Refs. 7-9, for example.) The mean steady flow is then described by a nonlinear equation for the zero incidence potential, and the unsteady flow is described by a linearized equation for the perturbed unsteady potential due to oscillation only, but with nonconstant coefficients determined by the mean steady flow. In this paper, the fundamental equations for the mean steady and unsteady flows, based on the unsteady full potential equation, were derived by using a body-normal coordinate system and are shown to be both of elliptic and hyperbolic equations, depending on the local mean steady flow Mach number. The numerical method of rotated difference scheme developed in Ref. 5 was used in solving both the mean steady (computer program RAXBOD) and unsteady flowfields. Harmonically pulsating and pitching oscillations are examined. Examples of the calculated results are given for both blunt and pointed bodies of revolution for quasisteady and unsteady flow conditions.

Presented as Paper 78-211 at the AIAA 16th Aerospace Sciences Meeting, Huntsville, Ala., Jan. 16-18, 1978; submitted Feb. 21, 1978; revision received Aug. 8, 1978.

Index categories: Transonic Flow; Nonsteady Aerodynamics; LV/M Aerodynamics.

*Research Engineer, Propulsion Wind Tunnel Facility, AEDC Division. Member AIAA.

II. Analysis

Basic Equations

The success of using a body-normal coordinate system with rotated difference scheme in predicting surface pressures of blunt and pointed bodies of revolution in steady transonic flow[5,6] prompts one to use the same approach for the calculation of unsteady surface pressure. The unsteady potential equation for an irrotational compressible fluid[10] is

$$\frac{1}{a^2}\cdot\frac{\partial^2\phi}{\partial t^2}+\frac{2}{a^2}q\cdot\frac{\partial q}{\partial t}=\nabla^2\phi-\frac{1}{a^2}q\cdot[(q\cdot\nabla)q] \tag{1}$$

where ϕ is the velocity potential, a is the speed of sound, q is the velocity vector, ∇ and ∇^2 are the divergent and Laplace operator, respectively, and t is the time. If Eq. (1) is applied to a body-normal coordinate system for a body of revolution at zero incidence, one obtains

$$\frac{1}{a^2}\cdot\frac{\partial^2\phi}{\partial t^2}+\frac{2}{a^2}\left[\frac{U}{H}\cdot\frac{\partial^2\phi}{\partial t\partial s}+V\frac{\partial^2\phi}{\partial t\partial n}+\frac{W}{r}\frac{\partial^2\phi}{\partial t\partial\psi}\right]$$

$$=\left(1-\frac{U^2}{a^2}\right)\frac{1}{H}\frac{\partial}{\partial s}\left(\frac{1}{H}\frac{\partial\phi}{\partial s}\right)+\left(1-\frac{V^2}{a^2}\right)\frac{\partial^2\phi}{\partial n^2}$$

$$+\left(1-\frac{W^2}{a^2}\right)\frac{1}{r^2}\cdot\frac{\partial^2\phi}{\partial\psi^2}-\frac{2}{a^2}\left(\frac{UV}{H}\cdot\frac{\partial^2\phi}{\partial s\partial n}+\frac{VW}{r}\cdot\frac{\partial^2\phi}{\partial n\partial\psi}\right.$$

$$+\frac{WU}{Hr}\frac{\partial^2\phi}{\partial s\partial\psi}\Big)+\Big(\frac{2UVK}{a^2H}+\frac{\sin\theta}{r}\Big)\frac{1}{H}\frac{\partial\phi}{\partial s}+\Big[\frac{K}{H}\Big(1-\frac{U^2}{a^2}\Big)$$

$$+\frac{\cos\theta}{r}\Big]\cdot\frac{\partial\phi}{\partial n}+\Big(\frac{V}{a}\cos\theta+\frac{U}{a}\sin\theta\Big)\frac{W}{ar^2}\cdot\frac{\partial\phi}{\partial\psi} \tag{2}$$

and

$$U=\cos\theta+\frac{1}{H}\cdot\frac{\partial\phi}{\partial s} \tag{3a}$$

$$V=-\sin\theta+\frac{\partial\phi}{\partial n} \tag{3b}$$

$$W=\frac{1}{r}\frac{\partial\phi}{\partial\psi} \tag{3c}$$

where U, V, and W are the axial, vertical, and circumferential velocity components, respectively, n and s are the body-normal and tangent coordiantes, ψ is the circumferential angle starting from the leeside plane of symmetry, K and θ are the curvature and inclination angles of body in the meridian plane, respectively, $H=1+Kn$, and r is the radial distance from the axis of symmetry. For flows about a body of revolution undergoing the small amplitude harmonic oscillation considered here, a $\cos\psi$ variation of the flow quantities in the ψ direction is assumed. It is also assumed that the solution can be expanded into a mean steady and an unsteady component[4]; for the latter, the time variation of the flow quantities is expressed by $e^{i\omega t}$; i.e.,

$$\phi=\phi_0(s,n)+\phi_1(s,n)\cos\psi e^{i\omega t} \tag{4}$$

where the subscripts 0 and 1 refer to the mean steady and unsteady components, respectively, and ω is the frequency of oscillations. Similar expressions can be made for U, V, and p.

By substituting Eq. (4) into Eq. (2) and collecting terms of the same order, one obtains the zeroth-order equation for ϕ_0 as follows:

$$\Big(1-\frac{U_0^2}{a_0^2}\Big)\frac{1}{H}\frac{\partial}{\partial s}\Big(\frac{1}{H}\frac{\partial\phi_0}{\partial s}\Big)-\frac{2U_0V_0}{a_0^2H}\frac{\partial^2\phi_0}{\partial s\partial n}$$

$$+\Big(1-\frac{V_0^2}{a_0^2}\Big)\frac{\partial^2\phi_0}{\partial n^2}+\Big[\frac{K}{H}\Big(1-\frac{U_0^2}{a_0^2}\Big)+\frac{\cos\theta}{r}\Big]\frac{\partial\phi_0}{\partial n}$$

$$+\Big[2\frac{KU_0V_0}{Ha_0^2}+\frac{\sin\theta}{r}\Big]\frac{1}{H}\frac{\partial\phi_0}{\partial s}=0 \tag{5}$$

and

$$U_0=\cos\theta+\frac{1}{H}\frac{\partial\phi_0}{\partial s} \tag{6a}$$

$$V_0=-\sin\theta+\frac{\partial\phi_0}{\partial n} \tag{6b}$$

The first-order equation for ϕ_1 is

$$-k^2\phi_1+\frac{2ik}{a_0^2}\Big[\frac{U_0}{H}\frac{\partial\phi_1}{\partial s}+V_0\frac{\partial\phi_1}{\partial n}\Big]=\Big(1-\frac{U_0^2}{a_0^2}\Big)\frac{1}{H}\frac{\partial}{\partial s}\Big(\frac{1}{H}\frac{\partial\phi_1}{\partial s}\Big)$$

$$+\Big(1-\frac{V_0^2}{a_0^2}\Big)\frac{\partial^2\phi_1}{\partial n^2}-\frac{C}{r^2}\phi_1-\frac{2U_0V_0}{a_0^2H}\frac{\partial^2\phi_1}{\partial s\partial n}$$

$$+\frac{A}{H}\frac{\partial\phi_1}{\partial s}+B\frac{\partial\phi_1}{\partial n} \tag{7}$$

where

$$A=\frac{2U_0V_0}{a_0^2H}+\frac{\sin\theta}{r}-\frac{2U_0}{a_0^2H}\frac{\partial}{\partial s}\Big(\frac{1}{H}\frac{\partial\phi_0}{\partial s}\Big)-2\Big(\frac{\partial^2\phi_0}{\partial s\partial n}\Big)\frac{V_0}{a_0^2}$$

$$+\Big(\frac{1}{H}\frac{\partial\phi_0}{\partial s}\Big)\frac{2KV_0}{a_0^2H}-\frac{K}{H}\frac{2U_0}{a_0^2}\Big(\frac{\partial\phi_0}{\partial n}\Big) \tag{8a}$$

$$B=\frac{K}{H}\Big(1-\frac{U_0^2}{a_0^2}\Big)+\frac{\cos\theta}{r}-\frac{2V_0}{a_0^2}\Big(\frac{\partial^2\phi_0}{\partial n^2}\Big)$$

$$-\frac{2U_0}{a_0^2}\Big(\frac{\partial^2\phi_0}{\partial s\partial n}\Big)+\frac{2KU_0}{a_0^2H}\Big(\frac{1}{H}\frac{\partial\phi_0}{\partial s}\Big) \tag{8b}$$

and

$$U_1=\frac{1}{H}\frac{\partial\phi_1}{\partial s} \tag{9a}$$

$$V_1=\frac{\partial\phi_1}{\partial n} \tag{9b}$$

The quantity C equals 0 or 1, depending on the type of flow under consideration. For axisymmetrical oscillatory flow, such as the pulsatile oscillation, ϕ_1 is independent of ψ; therefore, $\cos\psi$ should be replaced by unity in Eq. (4), and the term $(1/r^2\ \phi_1)$ should be eliminated from Eq. (7); that is, $C=0$. For a pitching oscillation, $C=1$. Since Eq. (7) is a complex equation ϕ_1 is a complex function and

$$\phi_1=\phi_{1R}(s,n)+i\phi_{1I}(s,n) \tag{10}$$

where the subscripts R and I stand for real and imaginary part, respectively. Consequently, U_1, V_1, and P_1 are all complex.

Boundary Conditions

The boundary condition is applied by requiring that the velocity vector be tangential to the surface, or

$$\frac{D\bar{B}}{Dt}=\frac{\partial\bar{B}}{\partial t}+U\frac{\partial\bar{B}}{\partial s}+V\frac{\partial\bar{B}}{\partial n}=0 \tag{11}$$

and

$$\bar{B}=n-n_1(s,t) \tag{12}$$

where n_1 is the perturbed body boundary due to motion. Thus the mean steady flow boundary condition is

$$V_0=\frac{\partial\phi_0}{\partial n}-\sin\theta=0 \tag{13}$$

and the perturbed unsteady flow boundary condition is

$$-\frac{\partial n_1}{\partial t}-U_0\frac{\partial n_1}{\partial s}+\frac{\partial\phi_1}{\partial n}=0 \tag{14}$$

The expressions for n_1 for two oscillatory motions which have engineering applications are now described.

1) Pulsatile oscillation with the amplitude proportional to the local radius:

$$n_1=\delta_0(r\cos\theta) \tag{15}$$

2) Pitching oscillation with amplitude τ_0:

$$n_1=\tau_0(d_t-Z)\cos\theta \tag{16}$$

where d_t is the pitch center and Z is the axial distance from the nose tip.

The boundary condition at the axis for axisymmetric flow is

$$\frac{\partial \phi_1}{\partial s} = 0 \tag{17a}$$

For nonaxisymmetric flow, one requires

$$\phi_1 = 0 \tag{17b}$$

because of the cosine variation of the flow in the crossflow plane.

Also, at infinity ($n \to \infty$), the velocity potential is required to vanish; that is $\phi_0 \to 0$ and $\phi_1 \to 0$.

Pressure Coefficients

The pressure coefficient C_p may be obtained by applying a perturbation approach to the unsteady Bernoulli equation, as follows:

$$C_{p_0} = \frac{2}{\gamma M_\infty^2}\left\{\left[1 - \frac{\gamma-1}{2} M_\infty^2 \left(1 - U_0^2 - V_0^2\right)\right]^{\gamma/(\gamma-1)} - 1\right\} \tag{18}$$

$$C_{p1R} + iC_{p1I} = -\frac{2}{\gamma M_\infty^2} \cdot \frac{\rho_0}{p_\infty}\left(\frac{\partial \phi_1}{\partial t} + \frac{U_0}{H}\frac{\partial \phi_1}{\partial s} + V_0 \frac{\partial \phi_1}{\partial n}\right) \tag{19}$$

where γ is the gas constant, ρ, p, and M are the density, pressure, and Mach number, respectively, and the subscript ∞ refers to the freestream condition.

III. Computational Scheme

The numerical method employed for the solution of the mean steady and unsteady flowfields is the same as that described in Ref. 5. In fact, the computer program RAXBOD developed by South at NASA Langley Research Center was used to solve the mean steady components, Eqs. (5) and (13). The unsteady components are given by Eqs. (7) and (14). It should be noted that Eq. (7) retains the same transonic flow characteristics of a mixed-type elliptic and hyperbolic differential equation, depending on whether the local mean steady flow is subsonic or supersonic. Hence, the scheme in Ref. 5 was applied to solve Eqs. (7) and (14). However, since Eqs. (7) and (14) are linear, the finite difference equations obtained are a set of linear algebraic equations and can be solved by a direct matrix inversion instead of a relaxation method, which was used in the solution of the mean steady flowfield.[5] The application of the rotated difference scheme to the perturbed flow, Eq. (7), and the boundary condition, Eq. (14), can be found in Ref. 11.

A computer program to solve for the perturbed flowfield was coded for an IBM 370-165 computer. The computational procedure is first to compute the mean steady flowfield using the computer program RAXBOD. The values of ϕ_0 in each node and other required information are stored, and then all the coefficients for the algebraic equation and the perturbed boundary conditions for a given oscillatory motion are computed. Once these computations are completed, a simultaneous solution of the algebraic equations gives the values of ϕ_{1R} and ϕ_{1I} at every nodal point. All perturbed flow quantities can now be obtained by differencing the terms ϕ_0, ϕ_{1R}, and ϕ_{1I}.

Regarding the selection of the nodal distribution to give good resolution, two sets of 97×33 and 97×97 were frequently used for the mean steady flow calculation. For the perturbed unsteady flow, four nodal distributions were tried (i.e., 25×9, 49×17, 97×17, and 97×33). The results obtained from 25×9 were not satisfactory in many cases, particularly at a supersonic freestream velocity. The results obtained from the 49×17, 97×17, and 97×33 matrices have good agreement in many cases. The required computer time is about 1½ min for 49×17, 4 min for 97×17, and 30 min for 97×33. It was decided that the nodal distribution of 97×17 is sufficiently good from the points of view of both accuracy and economy. Therefore, most results presented in this article are obtained using 97×17 nodes.

IV. Results and Discussions

Pulsatile Oscillation

A body of revolution undergoing oscillatory, pulsatile motion of the surface is a fundamental axisymmetric, unsteady motion. For the perturbation method developed in this article, the pulsatile oscillation can also provide a direct comparison between the quasisteady ($\omega = 0$) solution of the linear perturbed equation [Eq. (7)] and the steady-state solution to the nonlinear equation [identical to Eq. (5)] for the same body geometry. The case of a hemisphere-cylinder was chosen for comparison. The magnitude of the pulsatile oscillation is assumed to be proportional to 0.1 r, where r is the local radius of the body. As shown in Fig. 1, the expanded ($R_t = 1.1$) and the shrunken ($R_t = 0.9$) body is then an ellipse-cylinder with an axis ratio of 1.1 and 0.9, respectively, for the nose. The steady-state solution for the surface pressure for the ellipse-cylinders was obtained directly from the computer program RAXBOD shown by the solid curves in Fig. 2. The quasisteady solution for the same ellipse-cylinders can be obtained by adding (for $R_t = 1.1$) or subtracting (for $R_t = 0.9$) the perturbed pressure from the mean steady-state surface pressure for a hemisphere-cylinder ($R_t = 1.0$). The quasisteady solutions as shown by the broken curves in Fig. 1 are seen to agree well with the nonlinear solution.

Pitching Oscillation

Calculations for a pitching oscillation were performed for five body configurations: 1) 4-caliber ogive-nose-cylinder with $\ell/R = 20$; 2) 2-caliber ogive-nose-cylinder with $\ell/R = 14$; 3) 2:1 ellipse-nose-cylinder with $\ell/R = 20$; 4) hemisphere-cylinder with $\ell/R = 14$; and 5) parabolic arc nose with $\ell/R = 5$. The quasisteady solutions for the surface pressure will be compared to steady experimental data for configurations 1, 3, and 4 at zero and nonzero incidence. The quasisteady aerodynamic coefficients and the unsteady damping-in-pitch coefficients will be compared to experimental data and available theory for configurations 2, 4, and 5.

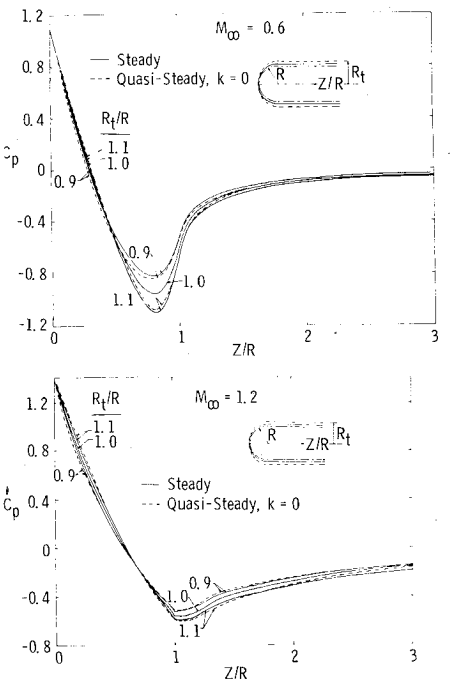

Fig. 1 Comparison of quasisteady and steady surface pressures about a hemisphere-cylinder undergoing pulsatile surface oscillations.

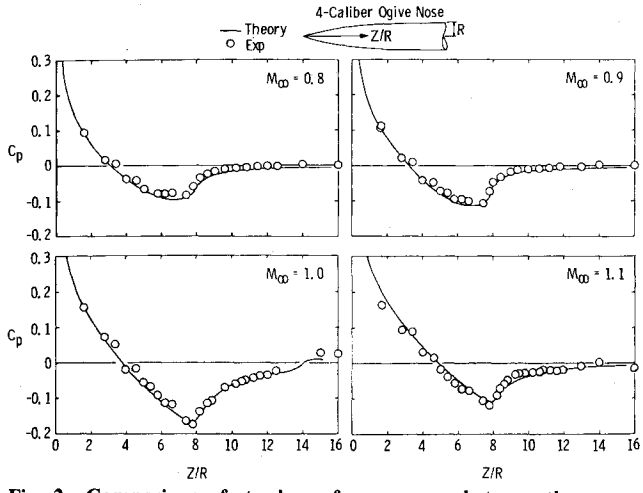

Fig. 2 Comparison of steady surface pressure between theory and experiments[12] for a 4-caliber ogive-nose-cylinder.

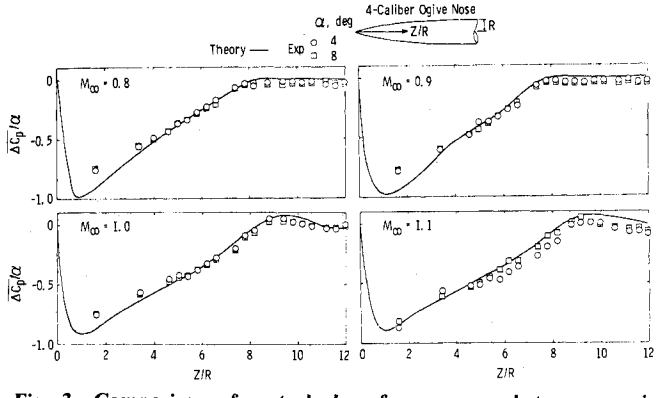

Fig. 3 Comparison of perturbed surface pressure between quasi-steady theory and experiments[12] for a 4-caliber ogive-nose cylinder.

Quasisteady Perturbation Pressure

4-Caliber Ogive-Nose-Cylinder

In Fig. 2, the steady-state solution of surface pressure for the 4-caliber ogive-nose-cylinder compares satisfactory with the experimental data[12] at zero incidence. Thus, the mean steady flow solution, which was used as the input for the unsteady flow calculation, is valid. The quasisteady solution for the perturbed surface pressure is shown in Fig. 3 for the leeward plane of symmetry. (All discussion in this article refers to the leeward plane of symmetry.) Since the perturbed flowfield is linear with respect to the incidence, the magnitude of $\overline{\Delta C_p}/\alpha$ is plotted. In Ref. 12, two sets of experimental data were obtained for $\alpha = \pm 4$ and ± 8 deg. To obtain the average perturbed pressure slope for comparison, the following formula was used

$$\overline{\Delta C_p}/\alpha = (C_{p_\alpha} - C_{p_{-\alpha}})/2\alpha$$

Figure 3 shows that the agreement between theory and experiment is excellent; the fact that the data for $\alpha = \pm 8$ and ± 4 deg agree very well, except at $M_\infty = 1.1$, indicates the linearity of the perturbed flow up to 8 deg.

2:1 Ellipse-Nose-Cylinder

In Fig. 4, the steady-state solutions for surface pressure ($M_\infty = 0.6$ to 1.2) for the 2:1 ellipse-nose-cylinder again compare satisfactorily with the experimental data of Ref. 12 at zero incidence. At incidence, the experimental data were obtained for $M_\infty = 0.9$ to 1.2 and $\alpha = \pm 8$ deg only. The comparison between the quasi-steady theory and experiments for the perturbed surface pressure in the leeward side ($\Delta C_p = C_{p_{\alpha=8\text{ deg}}} - C_{p_{\alpha=0}}$) and the windward side ($\Delta C_p = C_{p_{\alpha=0}} - C_{p_{\alpha=-8\text{ deg}}}$) is given in Fig. 5. The agreement is generally good; however, the theoretical data show a spike for $M_\infty = 0.9$ and a hump for $M_\infty \geq 1.0$ aft of the juncture of the ellipse and the cylinder. The cause may be attributed to the discontinuity in the curvature of the body geometry in the inviscid calculation of the perturbed flowfield. It is interesting to note that the experimental data for the windward side do show the type of peak (also a dip) for $M_\infty = 0.9$ and the hump for $M_\infty \geq 1.0$ in the approximate location given by the theory, but to a far lesser degree. The experimental data in the leeward side behave quite differently from the windward side in $2 < z/R < 2.5$ for M_∞ from 0.9 to 1.1 to indicate the effect of viscosity there and hence the deviation from the assumption of a $\cos\psi$ flowfield at $\alpha = 8$ deg.

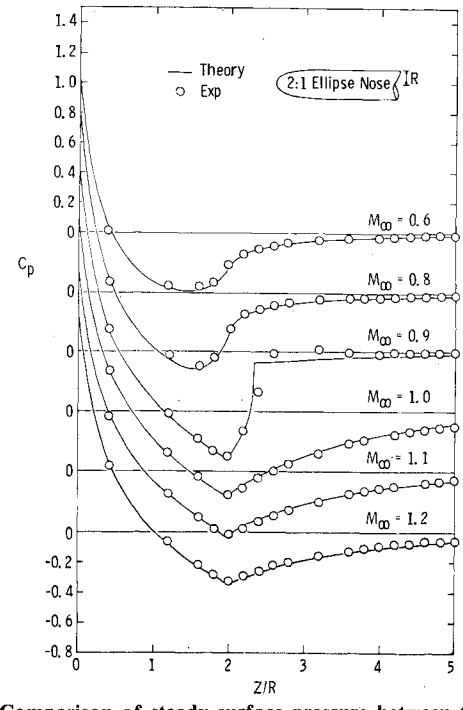

Fig. 4 Comparison of steady surface pressure between theory and experiments[12] for a 2:1 ellipse-nose-cylinder.

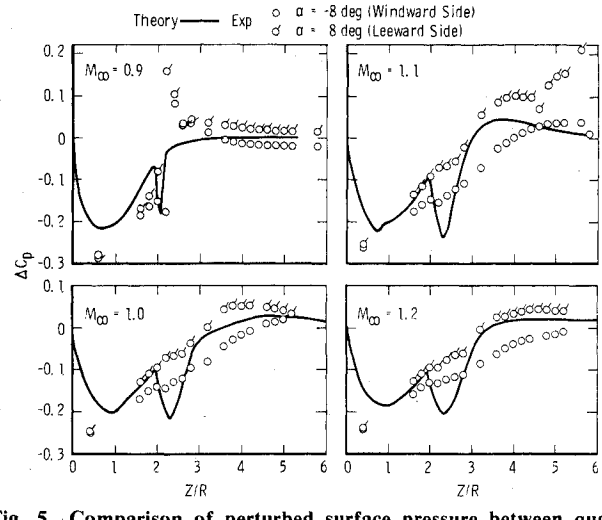

Fig. 5 Comparison of perturbed surface pressure between quasi-steady theory and experiments[12] for a 2:1 ellipse-nose-cylinder.

Hemisphere-Cylinder

The third configuration used for surface pressure comparison is a hemisphere-cylinder. A good agreement in the

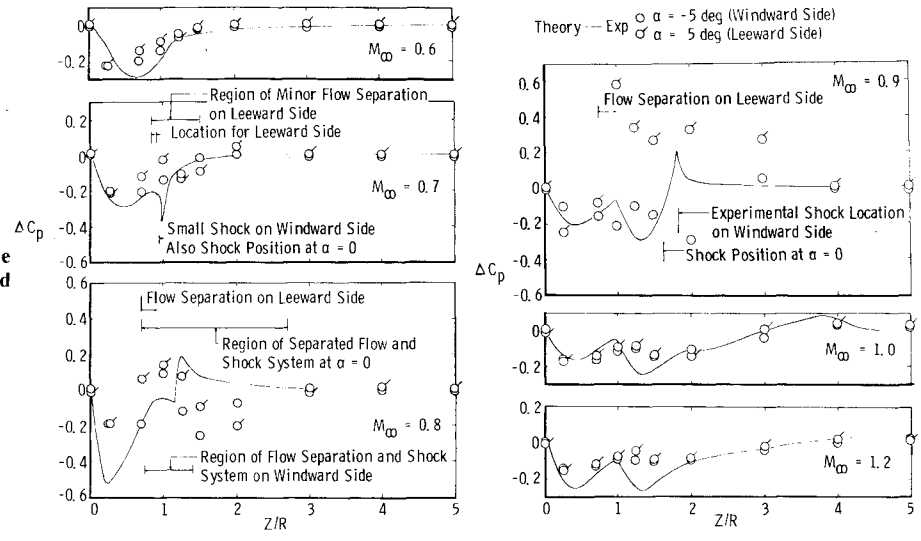

Fig. 6 Comparison of perturbed surface pressure between quasisteady theory and experiments[13] for a hemisphere-cylinder.

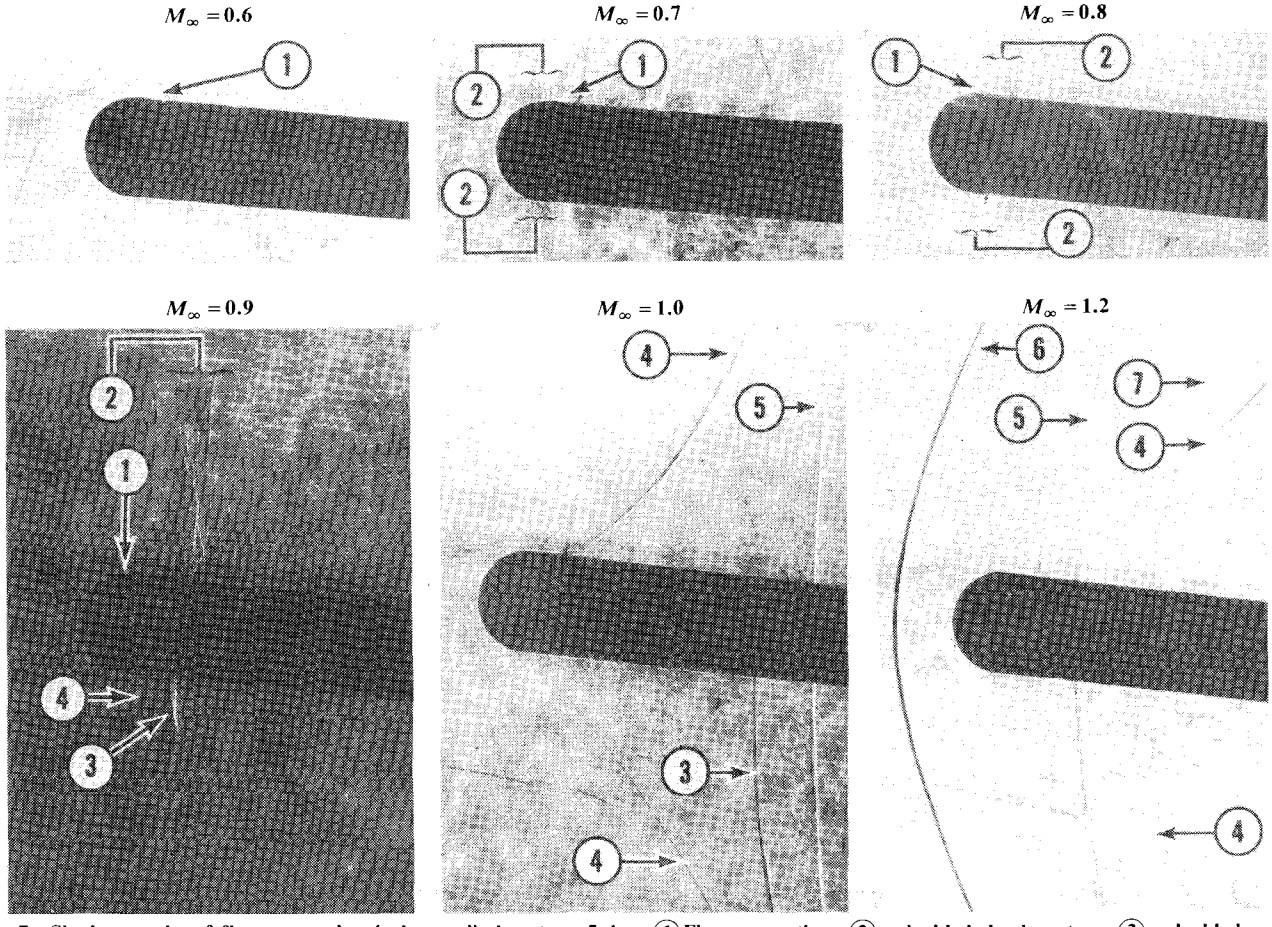

Fig. 7 Shadowgraphs of flow over a hemisphere-cylinder at $\alpha = 5$ deg. (1) Flow separation; (2) embedded shock system; (3) embedded normal shock; (4) recompression shock; (5) intersection of shock and tunnel sidewalls; (6) bow shock; (7) disturbances reflected from wall due to bow shock.

surface pressure between theory and experiments at zero incidence when there is no flow separation has been shown in Ref. 6. But flow separation does occur at M_∞ from 0.7 to 0.9 at zero incidence.[13] To evaluate the quasisteady theory at incidence, the experimental data for a hemisphere-cylinder at $\alpha = \pm 5$ deg contained in Ref. 13 were used. (In Ref. 13, $\psi = 0$ and 180 deg, which corresponds to $\alpha = 5$ and -5 deg, used here.) In Fig. 6, the leeward and windward side perturbation pressures are compared between theory and experiments for $M_\infty = 0.6$, 0.7, 0.8, 0.9, 1.0, and 1.2. Also, the shadowgraphs of the flowfield at $\alpha = 5$ deg are shown in Fig. 7. At $M_\infty = 0.6$, Fig. 7 shows that the flow is attached, except for a possible minor separation in the leeward side near the juncture of the hemisphere and the cylinder. This separation is also indicated by the experimental data of the perturbation pressure on the leeward and windward sides. The theory seems to slightly overpredict the perturbation pressure. For $M_\infty = 0.7$ to 0.9, Fig. 7 shows that the leeward flow separates. In the windward side, a small shock system indicated for $M_\infty = 0.7$; for $M_\infty = 0.8$, the shock system resembles the case of $\alpha = 0$, which indicates the existence of a separation bubble.[13] For $M_\infty = 0.9$, an embedded normal shock is shown. For the

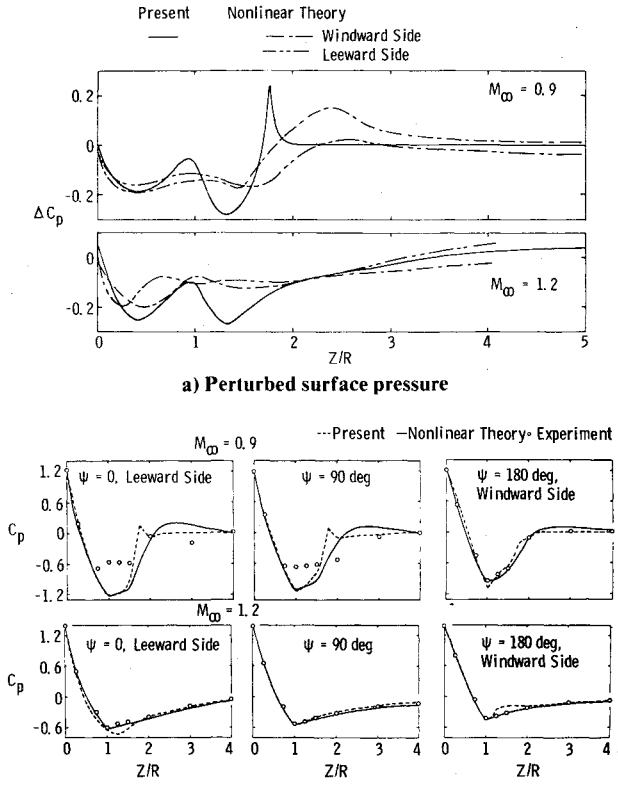

a) Perturbed surface pressure

b) Combined surface pressure

Fig. 8 Comparison of surface pressure between perturbation theory and nonlinear theory[13,14] for a hemisphere-cylinder at $\alpha = 5$ deg.

described flowfield, one would not expect good agreement between the theory and experiment due to the viscous effects. As shown in Fig. 6, the agreement is poor for these cases just discussed. For $M_\infty = 1.0$ and 1.2, Fig. 6 shows that the flow is again well attached, which is also indicated by the experimental data shown in Fig. 7. Thus for $M_\infty = 1.0$ and above, the comparison between theory and experiments is good except for the hump due to discontinuity in curvature aft of the juncture of the hemisphere and the cylinder, where the theory again shows a larger value.

Comparison with Nonlinear Theory

Inviscid nonlinear computations made by solving the Euler's equations are available for a hemisphere-cylinder at $\alpha = 5$ deg and $M_\infty = 1.2$[13] and $M_\infty = 0.9$.[14] In Fig. 8a, the perturbed surface pressure distributions are compared between the nonlinear theory and the present method. Since in Ref. 14 only the C_p values at $\psi = 0$, 90, and 180 deg were given, the C_p values at $\psi = 90$ deg were used to replace C_p values at $\alpha = 0$ to obtain the perturbed surface pressure. That is,

$$\text{windward side } \Delta C_p = C_{p_{\psi=180\,\text{deg}}} - C_{p_{\psi=90\,\text{deg}}}$$

$$\text{leeward side } \Delta C_p = C_{p_{\psi=90\,\text{deg}}} - C_{p_{\psi=0}}$$

The ΔC_p curves between the present calculation and the nonlinear theory agree well in the trend. It is also noted that at $\alpha = 5$ deg the assumption of $\cos\psi$ variation of flow variables in the present theory is perhaps invalid at the nose for $M_\infty = 1.2$ and at $1.5 < z/R < 3.0$ for $M_\infty = 0.9$.

A plot of the combined C_p for a hemisphere-cylinder at $\alpha = 5$ deg and $\psi = 0$, 90, and 180 deg is shown in Fig. 8b for $M_\infty = 0.9$ and 1.2. The agreement between present theory and the nonlinear theory is good except near the embedded shock region for $M_\infty = 0.9$ and aft of the juncture of the hemisphere and the cylinder for $M_\infty = 1.2$. The experimental data at $\psi = 0$ and 90 deg for $M_\infty = 0.9$ clearly show that the flow is separated in these two meridian planes.

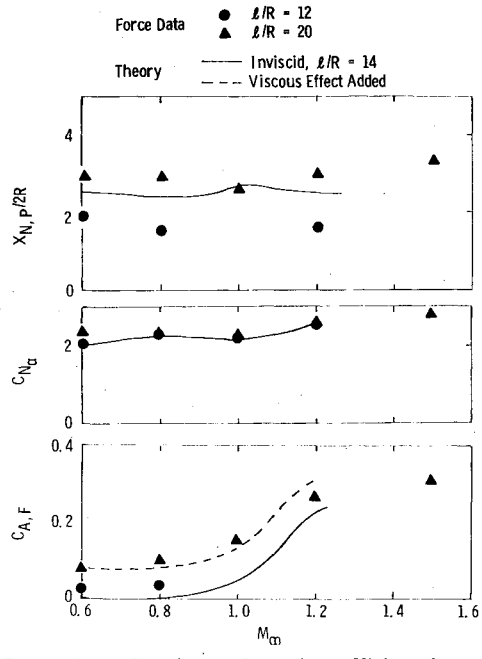

Fig. 9 Comparison of static aerodynamic coefficients between quasi-steady theory and experiments[15] for a 2-caliber ogive-cylinder.

Quasisteady Aerodynamic Coefficients

The integrated aerodynamic coefficients for the 2-caliber ogive-nose-cylinder and the hemisphere-cylinder are shown in Figs. 9 and 10, respectively. The experimental force data were obtained from Refs. 13 and 15. The theoretical value of $C_{A,F}$, the forebody axial-force coefficient, is the same as that at $\alpha = 0$ deg and is generally lower than that of the experiments. However, experimental force data for the shorter body and the integration of surface pressure measurements for the hemisphere-cylinder (Fig. 9) do show better agreement with the theory. This indicates that the difference is caused by the skin friction, which was not accounted for in the theory. When the viscous effect is added, using a skin friction corresponding to the experimental Reynolds number for the long body only, the agreement between theory and experiments for $C_{A,F}$ is excellent. The derivative of normal-force coefficients C_{N_α} is nearly independent of the body length and is shown to be in good agreement with the theory for the ogive-cylinder. For the hemisphere-cylinder, the hump and dip on the C_{N_α} data given by the theory between M_∞ from 0.6 to 0.9 was not shown by the experimental data; but for $M_\infty \geq 0.9$, the agreement is again good. The aerodynamic moment center (neutral point), $X_{N,P}$, measured from the body midpoint (positive forward) is compared between theory and experiments in Figs. 9 and 10, and the agreement is only fairly good.

Unsteady Calculations

Unsteady calculations were first performed for a parabolic arc nose at a reduced frequency of $k = \omega R/U_\infty = 0.006$, where R is the radius of the cylinder and $M_\infty = 1.0$. This case was computed by Liu and Ruo[2,16] by extending the parabolic method of Oswatisch and Keune.[17] The comparison of the stability derivatives of the total damping-in-pitch from the present theory and the theory of Liu and Ruo as well as the linearized theory of Laudahl (Fig. 12 of Ref. 16) for a variation in pitch center is shown in Fig. 11. It should be noted that Landahl's linearized theory is invalid for such low reduced frequency. Liu's theory indicates a reduction of the total damping-in-pitch coefficient when the nonlinearity of

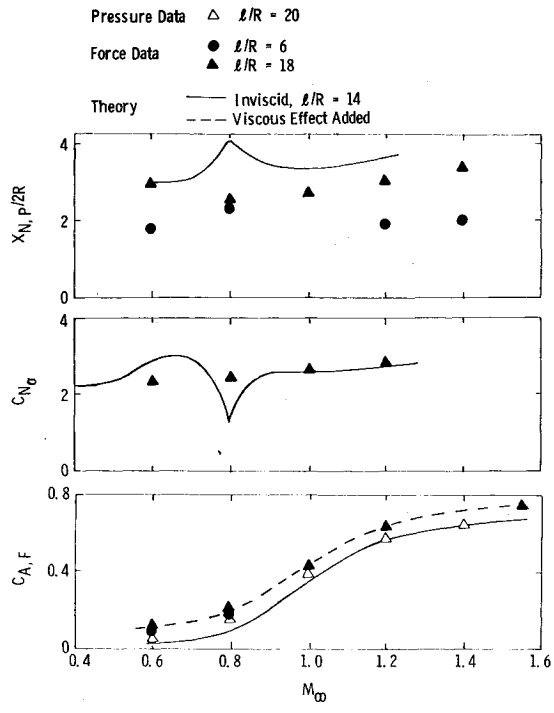

Fig. 10 Comparison of static aerodynamic coefficients between quasi-steady theory and experiments [13,15] for a hemisphere-cylinder.

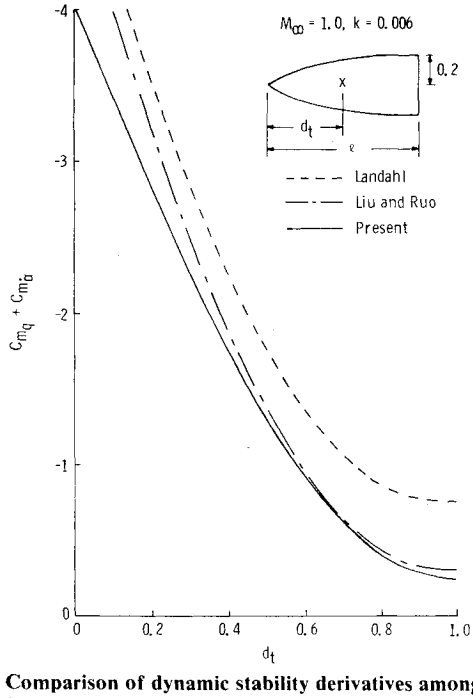

Fig. 11 Comparison of dynamic stability derivatives among theories as a function of pitching center for a parabolic arc nose.

the differential equation is approximately accounted for. The present theory indicates that the total damping-in-pitch coefficient is even lower. No experimental data are available for comparison.

No transonic unsteady surface pressure measurements for a body of revolution have been reported in the literature; therefore, a comparison of the unsteady surface pressure is not available. However, the stability derivative for total damping-in-pitch, $C_{m_{\dot\alpha}} + C_{m_q}$, has been reported in Refs. 18 and 19 for a 2-caliber-nose-ogive-cylinder and a hemisphere-cylinder. In these measurements, the models were pitched at a constant frequency of 36 Hz; hence the reduced frequency

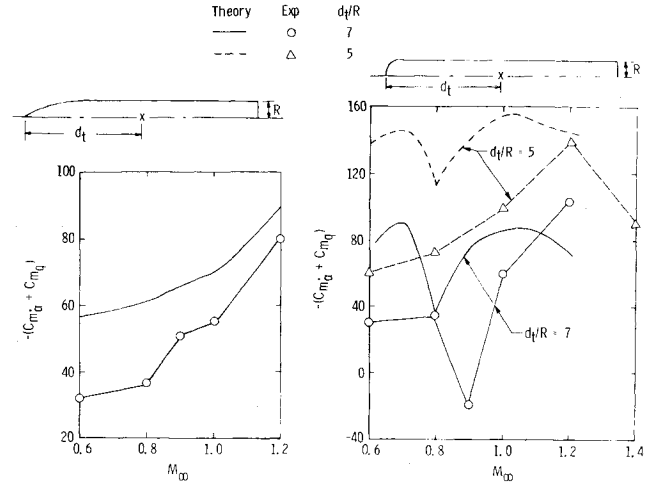

Fig. 12 Comparison of dynamic stability derivatives caused by pitching between theory and experiments. [18,19] a) 2-caliber ogive-nose-cylinder; b) hemisphere-cylinder.

changes with the freestream Mach number as follows:

$M_\infty = 0.6 \quad 0.7 \quad 0.8 \quad 0.9 \quad 1.0 \quad 1.1 \quad 1.2$

$k = .0165 \quad .0145 \quad .0124 \quad .0112 \quad .0099 \quad .0095 \quad .0088$

Calculations were made using the corresponding reduced frequency for each Mach number. Figure 12 shows the stability derivatives for total damping-in-pitch for the ogive-cylinder and the hemisphere-cylinder. For the ogive-cylinder the $C_{m_{\dot\alpha}} + C_{m_q}$ value given by the theory is generally higher than the experimental data, particularly for the lower Mach number. For the hemisphere-cylinder, the experimental data for $d_t/R = 7$ were obtained from Ref. 18 for the full-span model; data for $d_t/R = 5$ were from Ref. 19. The agreement between theory and experiment is not satisfactory. The theoretical calculations were made for $M_\infty = 0.6, 0.7, 0.8, 0.9, 1.0$, and 1.2 to determine the curves, which shows the general trend given by the experimental data. For example, the experimental data for $d_t/R = 7$ show a dip at $M_\infty = 0.9$ which corresponds to the dip given by the theory at $M_\infty = 0.8$ and the set of data for $d_t/R = 5$ also indicates a drop of $C_{m_{\dot\alpha}} + C_{m_q}$ at $M_\infty = 1.4$ as given by the theory. However, the experiments for $d_t/R = 7$ gave a positive value of $C_{m_{\dot\alpha}} + C_{m_q}$ (unstable) at $M_\infty = 0.9$ which was not predicted by the theory. As pointed out previously, for a hemisphere-cylinder in the transonic flow regime, the flowfield is complicated by the viscous and inviscid interaction. Therefore, inviscid theory may not be sufficient to predict the dynamic stability derivatives.

V. Conclusions

A perturbation theory and numerical solution based on the unsteady full potential equation were developed for unsteady transonic flow about blunt and pointed bodies of revolution undergoing harmonic oscillations. Calculations were performed for ogive-cylinder, ellipse-cylinder, hemisphere-cylinder, and parabolic arc nose shapes undergoing pulsatile and pitching oscillations. The following conclusions can be drawn.

1) The quasisteady solutions for the perturbation surface pressure for bodies of revolution of small incidence agree well with the experiments, particularly for the pointed-nose body of revolution. For blunt-nose bodies of revolution, the discontinuity of curvature of the body geometry causes local deviation of surface pressure between theory and experiments.

2) For blunt-nose bodies of revolution in the transonic Mach number range, the flow is separated in the leeward side even at small incidence; thus the inviscid theory and the

assumption of cosine variation of flow quantities in the crossflow plane become invalid.

3) The total surface pressure predicted by the perturbation theory compares favorably with nonlinear theory (solution to Euler's equation) for a hemisphere-cylinder at $\alpha = 5$ deg and $M_\infty = 0.9$ and 1.2.

4) The agreement between the present theory and the experiments is good for the total normal-force coefficient, except for the hemisphere-cylinder at $M_\infty = 0.6$ to 0.8, and for the forebody axial-force coefficient (with skin-friction correction); the predicted center of pressure is only fairly good.

5) The unsteady results for the total damping-in-pitch coefficient agree well with the available calculation for a parabolic arc nose. The predicted total damping-in-pitch coefficients for a 2-caliber ogive-nose-cylinder and a hemisphere-cylinder do not agree well with the limited experimental data. More experimental data, particularly unsteady surface pressure data, are needed to evaluate the present theory and for future theoretical development.

Acknowledgment

The research reported herein was performed by the Arnold Engineering Development Center, Air Force Systems Command. Work and analysis for this research was done by personnel of ARO, Inc., a Sverdrup Corporation Company, operating contractor of AEDC. Further reproduction is authorized to satisfy needs of the U.S. Government. The assistance of G. Lewis in computing the results is gratefully acknowledged.

References

[1] Landahl, M. L., *Unsteady Transonic Flow*, Pergamon Press, New York, 1961.

[2] Liu, D. D., Platzer, M. F., and Ruo, S. Y., "Unsteady Linearized Transonic Flow Analysis for Slender Bodies," *AIAA Journal*, Vol. 15, July 1977, pp. 966-973.

[3] Kimble, K. R., Liu, D. D., Ruo, S. Y., and Wu, J. M., "Unsteady Transonic Flow Analysis for Low Aspect Ratio, Pointed Wings," *AIAA Journal*, Vol. 12, April 1974, pp. 516-522.

[4] Stahara, S. S. and Spreiter, J. R., "Unsteady Local Linearization Solution for Pitching Bodies of Revolution at Freestream Mach Numbers = 1: Stability Derivative Analysis," *AIAA Journal*, Vol. 14, Oct. 1976, pp. 1402-1408.

[5] South, J. C. and Jameson, A., "Relaxation Solutions for Inviscid Axisymmetric Transonic Flow Over Blunt or Pointed Bodies," *Proceedings of AIAA Computational Fluid Dynamics Conference*, July 1973, pp. 8-17.

[6] Hsieh, T., "Flow Field Study about a Hemisphere-Cylinder in Transonic and Low Supersonic Mach Number Range," AIAA Paper 75-83, Jan. 1975; also *AIAA Journal*, Vol. 13, Dec. 1975, pp. 1411-1413.

[7] Traci, R. M., Albano, E. D., and Farr, J. L., Jr., "Perturbation Method for Transonic Flows about Oscillating Airfoils," *AIAA Journal*, Vol., 14, Sept. 1976, pp. 1258-1265.

[8] Ehlers, F. E., "A Finite Difference Method for the Solution of the Transonic Flow Around Harmonically Oscillating Wings," AIAA Paper 74-543, June 1974.

[9] Chan, S. T. K. and Chen, H. C., "Finite Element Applications to Unsteady Transonic Flow," AIAA Paper 77-446, March 1977.

[10] Pai, S. I., *Introduction to the Theory of Compressible Flow*, Van Nostrand Company, Inc., Princeton, N.J., 1959.

[11] Hsieh, T., "Unsteady Transonic Flow Over Blunt and Pointed Bodies of Revolution," AEDC-TR-77-100, Feb. 1978.

[12] Hartley, M. S. and Jacocks, J. L., "Static Pressure Distributions on Various Bodies of Revolution at Mach Numbers from 0.6 to 1.6," AEDC-TR-68-37 (AD828571), March 1968.

[13] Hsieh, T., "An Investigation of Separated Flow about a Hemisphere-Cylinder at 0- to 19-deg Incidence in the Mach Number Range from 0.6 to 1.5," AEDC-TR-76-112, Nov. 1976.

[14] Pulliam, T. H. and Steger, J. L., "On Implicit Finite-Difference Simulations of Three Dimensional Flow," AIAA Paper 78-10, Jan. 1978.

[15] Anderson, C. F. and Henson, J. R., "Aerodynamic Characteristics of Several Bluff Bodies of Revolution at Mach Numbers from 0.6 to 1.5," AEDC-TR-71-130 (AD885911), July 1971.

[16] Ruo, S. Y. and Liu, D. D., "Calculation of Stability Derivatives for Slowly Oscillating Bodies of Revolution at Mach 1.0," Huntsville Research and Engineering Center, Lockheed Missile and Space Company, Inc., Huntsville, Ala., HREC-0082-24, Feb. 1971.

[17] Oswatisch, K. and Keune, F., "Flow Around Bodies of Revolution at Mach Number One," *Proceedings of the Conference on High-Speed Aeronautics*, Polytechnic Institute, 1955.

[18] Shadow, T. O., "An Investigation of the Half-Model Reflection-Plane Technique for Dynamic Stability Testing at Transonic Mach Numbers," AEDC-TR-76-165 (ADA035567), Jan. 1977.

[19] Shadow, T. O. and Paulk, R. A., "Dynamic Stability Characteristics of Bluff Bodies of Revolution at Transonic Mach Numbers," AEDC-TR-72-100 (AD902214L), Aug. 1972.